

CAN MOLECULAR FOUNDATION MODELS KNOW WHAT THEY DON'T KNOW? A SIMPLE REMEDY WITH PREFERENCE OPTIMIZATION

Langzhou He¹, Junyou Zhu^{2,3}, Fangxin Wang¹, Junhua Liu⁴,
Haoyan Xu⁴, Yue Zhao⁴, Philip S. Yu¹, Qitian Wu^{5*}

¹University of Illinois Chicago ²Potsdam Institute for Climate Impact Research

³Technical University of Berlin ⁴University of Southern California

⁵Broad Institute of MIT and Harvard

{lhe24, fwang51, psyu}@uic.edu {haoyanxu, yzhao010, jliu2321}@usc.edu
junyou.zhu@pik-potsdam.de wuqitian@broadinstitute.org

ABSTRACT

Molecular foundation models are rapidly advancing scientific discovery, but their unreliability on out-of-distribution (OOD) samples severely limits their application in high-stakes domains such as drug discovery and protein design. A critical failure mode is chemical hallucination, where models make high-confidence yet entirely incorrect predictions for unknown molecules. To address this challenge, we introduce *Molecular Preference-Aligned Instance Ranking* (Mole-PAIR), a simple, plug-and-play module that can be flexibly integrated with existing foundation models to improve their reliability on OOD data through cost-effective post-training. Specifically, our method formulates the OOD detection problem as a preference optimization over the estimated OOD affinity between in-distribution (ID) and OOD samples, achieving this goal through a pairwise learning objective. We show that this objective essentially optimizes AUROC, which measures how consistently ID and OOD samples are ranked by the model. Extensive experiments across five real-world molecular datasets demonstrate that our approach significantly improves the OOD detection capabilities of existing molecular foundation models, achieving up to **45.8%**, **43.9%**, and **24.3%** improvements in AUROC under distribution shifts of size, scaffold, and assay, respectively.

1 INTRODUCTION

Artificial intelligence has enabled major advances in fields such as drug discovery (David et al., 2020) and materials science (Sanchez-Lengeling et al., 2017). Molecular foundation models, pre-trained on large chemical datasets, have shown strong potential to accelerate molecular design by predicting physicochemical and biological properties with improved accuracy (Beaini et al., 2023; Méndez-Lucio et al., 2024; Luo et al., 2023). Despite this promise, a central barrier to their deployment in industrial pipelines is the reliability of their predictions (Jiang et al., 2024; Wang et al., 2024). Without robust confidence estimation, these models may produce misleading outputs.

A key manifestation of this issue is *chemical hallucination*, analogous to hallucination observed in modern large language models (Xu et al., 2025). This problem is particularly severe for out-of-distribution (OOD) molecules (Liang et al., 2017), which deviate significantly from the training distribution. In such cases, models often generate incorrect predictions with high confidence, such as falsely assigning strong bioactivity to an inactive or toxic compound. These failures can have substantial consequences: confidently mispredicting the activity of a novel scaffold may lead to wasted investment in synthesis and testing (Ramsundar et al., 2017), while overlooking an activity cliff—where a small structural change causes a sharp loss of activity (Maggiora, 2006)—can misdirect optimization efforts in drug discovery and designs (van Tilborg et al., 2022).

*Corresponding author.

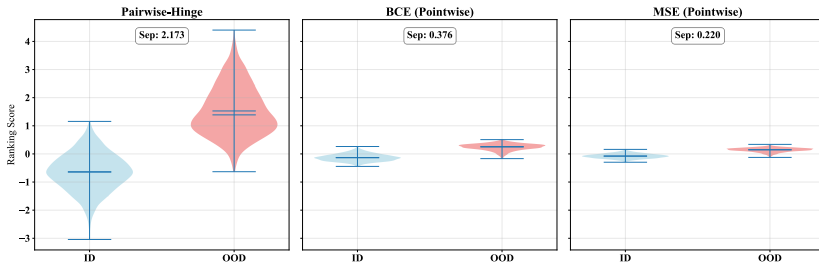


Figure 1: A case study illustrating the objective-metric misalignment. The figure plots the estimated OOD affinity scores yielded by the model trained with different objectives for ID and OOD samples on the IC50-Scaffold task. The Pairwise-Hinge loss (Joachims, 2002) produces a globally separated score distribution between ID and OOD, aligning with AUROC, whereas the two pointwise objectives yield heavily overlapping scores due to their per-sample calibration loss. This clearly demonstrates the importance of objective-metric alignment for OOD detection.

While there are many existing efforts on addressing OOD detection in molecular data or graph data more broadly (Li et al., 2022; Wu et al., 2024; Bao et al., 2024), most of these approaches are tied to specific architectures such as particular graph-based generative models (Liu et al., 2023; Wu et al., 2023) or are directly adapted from images to molecules (Du et al., 2023; Shen et al., 2024; Wang et al., 2025a), which either limits their wide applicability or lacks specific domain knowledge. Furthermore, to the best of our knowledge, the common design of these approaches resorts to pointwise estimation and optimization, where each data sample is allocated with a scalar output indicating its affinity to OOD samples and the models are trained with regression-style objectives (Hendrycks & Gimpel, 2016; Liang et al., 2017; Liu et al., 2020; Lee et al., 2018; Sun et al., 2022; Breunig et al., 2000; Li et al., 2025; Zhu et al., 2025). However, this would lead to mismatch with the desired evaluation metric (e.g., AUROC), which seeks the consistent ranking between OOD and ID samples (Figure 1 provides concrete evidence for this issue on real-world data).

To fill this research gap, in this paper, we propose to formulate the OOD detection problem as a preference optimization problem which aims at preserving the correct ranking between any pair of OOD and ID samples. To achieve this goal, we devise a pairwise learning objective, Mole-PAIR, that is agnostic to model architectures and directly optimizes the estimated OOD affinity, without requiring class logits or property labels. Notably, this plug-and-play approach can be seamlessly integrated with arbitrary off-the-shelf molecular foundation models to enhance their OOD detection capability through cost-effective post-training that trains only a lightweight detector. As justification for this design, we prove that this new objective essentially optimizes the AUROC, which measures the consistency of the estimated OOD affinity across any pair of OOD and ID samples. We apply this approach to five public molecular datasets and compare it with recently proposed methods under diverse benchmarking settings including three types of distribution shifts and two recently proposed molecular foundation models (MiniMol (Kläser et al., 2024) and Uni-mol (Zhou et al., 2023; Lu et al., 2024)). The results show that our approach yields consistent improvements across multiple performance metrics, with average gains of 28.3% on AUROC, 28.5% on AUPR, and 25.3% on FPR95 across all datasets.

Our main contributions are summarized below:

- We formulate out-of-distribution detection as a preference optimization problem, where the detector targets consistent ranking of the estimated OOD affinity between in-distribution and out-of-distribution samples. This is achieved by a proposed pairwise learning objective that, as demonstrated by our theoretical analysis, inherently optimizes the AUROC quantifying the ranking consistency across any pair of ID and OOD data.
- On top of this new objective, we frame the proposed approach as a plug-and-play, model-agnostic framework for enhancing the OOD detection capability of molecular foundation models through cost-effective post-training (that does not update the main parameters of pretrained models). This leads to a flexible, lightweight and universal approach for improving the reliability of existing foundation models in molecule-related tasks.

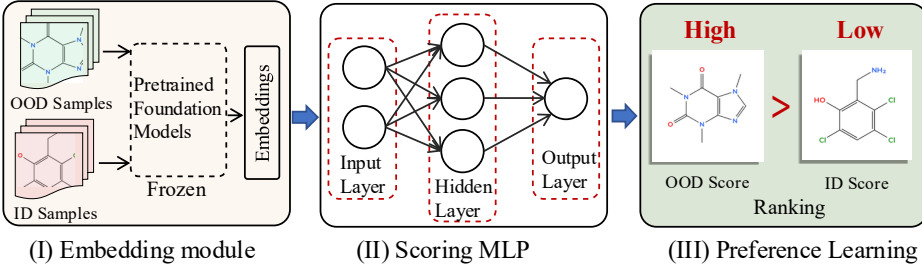


Figure 2: Overview of the Mole-PAIR framework.

- We conduct comprehensive experiments on multiple challenging molecular OOD benchmarks (DrugOOD (Ji et al., 2022) and GOOD (Gui et al., 2022)) that involve diverse distribution shifts. The results consistently show that Mole-PAIR significantly outperforms recently proposed approaches for OOD detection as measured by AUROC, AUPR, and FPR95, with an average of 28.3% AUROC increase across five datasets and reduction of FPR95 to zero in quite a few cases.

2 RELATED WORK

General OOD Detection OOD detection has attracted wide attention due to the increasing need for building reliable AI. Early approaches such as One-Class SVM (Schölkopf et al., 1999), LOF (Breunig et al., 2000), and Isolation Forest (Liu et al., 2008) operate under Euclidean feature spaces and the i.i.d. assumption. In the deep learning era, widely used generic OOD post-hoc methods include MSP (Hendrycks & Gimpel, 2016) relying on maximum softmax probability, ODIN (Liang et al., 2017) employing temperature scaling and small input perturbations, Mahalanobis distance (Lee et al., 2018) adopting class-conditional Gaussian features, and Deep KNN (Sun et al., 2022), a nonparametric nearest-neighbor detector in the deep feature space. However, these methods are tied to Euclidean embeddings and a softmax classifier head, and they are mostly evaluated on vision benchmarks, which limits their transferability and generalizability to chemistry-constrained molecular graphs and regression tasks.

OOD Detection for Molecules Graph-based models are widely used because many real-world problems involve non-Euclidean relational data, and this has sparked diverse graph OOD detection methods (Li et al., 2022; Guo et al., 2023). These approaches often rely on techniques such as energy-based scoring (Wu et al., 2023), analysis of topological properties (Bao et al., 2024), or synthesis-based OOD generation (Wang et al., 2025a). However, as they are designed for general graphs, these methods often lack domain-specific chemical or molecular knowledge. In contrast, methods that are developed specifically for molecular OOD detection tend to be tightly coupled with specific model architectures and training pipelines, such as reconstruction-similarity with diffusion models for molecules (Shen et al., 2024). This integration makes them less adaptable for use with diverse, pre-trained molecular foundation models, highlighting a need for more flexible solutions.

AI Reliability A key direction for improving AI reliability is to equip pre-trained models with mechanisms to manage predictive uncertainty, especially without costly retraining. Existing post-hoc methods, such as Conformal Prediction and Selective Prediction, focus on managing uncertainty for ID data (Lei et al., 2018; Romano et al., 2020; Lin et al., 2023; Rong et al., 2020; Wang et al., 2025b). Conformal Prediction calibrates a model’s scores to produce prediction sets that provably contain the true label with a user-specified frequency, offering distribution-free coverage guarantees for ID samples (Angelopoulos et al., 2022; Laghuvarapu et al., 2023; Arvidsson McShane et al., 2024). Selective Prediction equips a model with a reject option, allowing it to abstain on low-confidence inputs to control the error rate on the predictions it chooses to make (Geifman & El-Yaniv, 2017; 2019; Guo et al., 2017). While they can react to OOD samples, their main goal is to control error rates and manage risk on ID data. In contrast, the fundamental goal of OOD detection is to explicitly identify and flag inputs that originate from a different distribution than the one the model was trained on.

3 METHODOLOGY

In this section, we introduce ***Molecular Preference-Aligned Instance Ranking*** (Mole-PAIR), a post-training approach for enhancing the OOD detection capability of molecular foundation models. Our approach casts OOD detection as preference learning and optimizes a pairwise ranking objective that aligns with optimizing the AUROC between ID and OOD samples. Figure 2 shows the workflow of our proposed model.

3.1 OUT-OF-DISTRIBUTION DETECTION FOR MOLECULES

Problem Formulation. We consider an input molecule represented by its SMILES string $S \in \mathcal{S}$. We use MiniMol (2D) (Kläser et al., 2024) and Uni-Mol (3D) (Zhou et al., 2023; Lu et al., 2024) to generate molecular embeddings. MiniMol converts the SMILES string into a 2D molecular graph that represents atomic connectivity. This graph, which contains features for atoms and bonds, is then processed by a GNN to produce a final embedding that captures the molecule’s topological structure. Unimol first generates the molecule’s 3D spatial structure from the SMILES string, then uses a transformer-based model to take these 3D coordinates as input to learn a representation that encodes the molecule’s geometric shape and spatial properties. The training dataset is divided into an in-distribution subset $D_{\text{in}}^{\text{train}}$ drawn from D_{in} and an out-of-distribution subset $D_{\text{out}}^{\text{train}}$ drawn from D_{out} , while at test time we evaluate on D^{test} , which is similarly partitioned into $D_{\text{in}}^{\text{test}}$ and $D_{\text{out}}^{\text{test}}$.

For the OOD detection task, we aim to design a detector g that decides whether a given molecule S is from in-distribution (ID) or out-of-distribution (OOD):

$$g(S; \tau, E_\phi) = \begin{cases} 1 & (\text{ID}), \quad \text{if } E_\phi(S) < \tau, \\ 0 & (\text{OOD}), \quad \text{if } E_\phi(S) \geq \tau, \end{cases} \quad (1)$$

where $E_\phi(\cdot)$ is a learnable detector and τ is a decision threshold. The score from $E_\phi(S)$ indicates the OOD affinity of the sample S estimated by the model. The ideal detector should satisfy $E_\phi(S_{\text{in}}) < E_\phi(S_{\text{out}})$ for all $S_{\text{in}} \sim D_{\text{in}}$ and $S_{\text{out}} \sim D_{\text{out}}$.

OOD Detector for Foundation Models. Without loss of generality, we consider a molecular foundation model f_{Encoder} that maps any input molecule S to an embedding vector in latent space:

$$h = f_{\text{Encoder}}(S) \in \mathbb{R}^p. \quad (2)$$

We compose the scoring function E_ϕ from a frozen, pre-trained f_{Encoder} and a trainable head g_{Head} :

$$E_\phi(S) = g_{\text{Head}}(f_{\text{Encoder}}(S); \phi), \quad (3)$$

where the trainable parameters ϕ consist only of those in g_{Head} while the parameters of f_{Encoder} are frozen. This plug-in design focuses post-training on the OOD scoring function (also known as the detector) and is compatible with any off-the-shelf molecular foundation models.

3.2 PREFERENCE OPTIMIZATION LEARNING OBJECTIVE

Achieving the goal of $E_\phi(S_{\text{in}}) < E_\phi(S_{\text{out}})$ is non-trivial since such a target involves the ranking between any pair of ID and OOD samples. A quantitative metric for measuring how close the ranking yielded by the model’s estimation is to the ideal case is the Area Under the Receiver Operating Characteristic Curve (AUROC) that equals the probability that for any pair of ID and OOD samples how likely the ID sample is ranked before the OOD one:

$$\text{AUROC} = \Pr(E_\phi(S_{\text{in}}) < E_\phi(S_{\text{out}})), \quad S_{\text{in}} \sim D_{\text{in}}^{\text{test}}, \quad S_{\text{out}} \sim D_{\text{out}}^{\text{test}}. \quad (4)$$

The ideal learning objective for OOD detection should maximize the AUROC produced by the model’s estimated OOD affinity.

Preference Optimization for OOD Detection. Directly optimizing AUROC is intractable due to the non-differentiability. In this work, we resort to a pairwise learning objective inspired by direct preference optimization (DPO) (Rafailov et al., 2024) that has shown success in post-training modern large language models (LLMs) (Wang et al., 2023; Tunstall et al., 2023; Hong et al., 2024; Meng

et al., 2024). The main idea of DPO is to learn directly from pairwise preferences with a simple logistic likelihood, without training a separate reward model or using on-policy reinforcement learning for LLM post-training. We extend this principle for post-training molecular foundation models for OOD detection, where, in particular, we replace the LLM policy score with the estimated OOD affinity $E_\phi(S)$ produced by the detector head on top of a frozen encoder, and use only the pairwise ranking labels for optimization. Specifically, following the Bradley–Terry model (Bradley & Terry, 1952), we introduce a pairwise learning objective that imposes the target that for any pair of ID and OOD samples, the ID sample is preferred:

$$P(S_{\text{in}} \succ S_{\text{out}}) = \sigma(\beta \cdot [E_\phi(S_{\text{out}}) - E_\phi(S_{\text{in}})]), \quad (5)$$

where $\sigma(u) = (1 + e^{-u})^{-1}$ is the logistic sigmoid that converts the detector margin $\Delta E_\phi = E_\phi(S_{\text{out}}) - E_\phi(S_{\text{in}})$ into a probability in $[0, 1]$. The larger the margin, the closer this probability is to 1, indicating stronger confidence that the ID sample should be ranked before the OOD sample. The temperature parameter $\beta > 0$ adjusts how sensitive the probability is to the margin: a larger β makes the model react more strongly to small differences, whereas a smaller β yields more gradual training signals. Maximizing the log-likelihood over pairs yields the **Mole-PAIR loss**:

$$\mathcal{L}_{\text{Mole-PAIR}}(\phi) = -\mathbb{E}_{S_{\text{in}} \sim D_{\text{in}}, S_{\text{out}} \sim D_{\text{out}}} [\log \sigma(\beta \cdot [E_\phi(S_{\text{out}}) - E_\phi(S_{\text{in}})])]. \quad (6)$$

In practice we construct balanced mini-batches of ID and OOD samples and compute margins within the batch to estimate the expectation efficiently. This focuses learning on relative ranking rather than absolute scores and is consistent with optimizing AUROC (see more justification in Sec. 4).

Regularization. Since AUROC depends only on the ordering of scores and the loss function Eq. (6) depends only on the margin, adding a constant offset to the detector output does not change the overall trend. Thus, the training objective is invariant to global translations $E_\phi(S) \mapsto E_\phi(S) + c$, which can cause scale drift and numerical instability. To fix this gauge and stabilize the scale without affecting the optimal ranking, we add a small ℓ_2 penalty on the detector output:

$$\mathcal{L}_{\text{total}}(\phi) = \mathcal{L}_{\text{Mole-PAIR}}(\phi) + \lambda (\mathbb{E}[E_\phi(S_{\text{in}})^2] + \mathbb{E}[E_\phi(S_{\text{out}})^2]), \quad \lambda > 0 \text{ small.} \quad (7)$$

This penalty anchors the mean OOD affinity near zero and discourages unnecessarily large magnitudes, preventing saturation of the loss function when $\beta \Delta E_\phi$ becomes too large. At test time we use $E_\phi(S)$ as the OOD affinity (higher means more OOD-like) and evaluate the model with multiple threshold-free metrics including AUROC on $(D_{\text{in}}^{\text{test}}, D_{\text{out}}^{\text{test}})$.

4 THEORETICAL DISCUSSIONS

In this section, we provide the theoretical justification for Mole-PAIR and show that our preference-based framework is formally principled. To begin with, we clarify the mismatch between traditional point-wise estimation and the desired evaluation metric in OOD detection. What OOD detection ultimately evaluates is a ranking: the AUROC equals $\Pr(E_\phi(S_{\text{in}}) < E_\phi(S_{\text{out}}))$ (Fawcett, 2006; Cortes & Mohri, 2003), i.e., how often ID scores rank below OOD scores. Pointwise objectives such as using MSE or BCE to regress a single scalar score assume absolute calibration, which is fragile under distribution shifts and orthogonal to AUROC’s relative nature. Mole-PAIR instead trains on pairwise ID–OOD comparisons via the logistic loss in Eq. 6 and the total objective in Eq. 7. During training, the encoder used for molecular embeddings stays frozen and we only learn a small ranking score head $E_\phi(\cdot)$, which makes post-training lightweight and property-label free. Notation, assumptions, and the full objective are summarized in Appendix A.1.

4.1 ADAPTIVE LEARNING BY PRIORITIZING HARD PAIRS

We now unpack what this loss optimizes in practice. For any ID–OOD pair $(S_{\text{in}}, S_{\text{out}})$, we define:

$$\Delta E_\phi = E_\phi(S_{\text{out}}) - E_\phi(S_{\text{in}}). \quad (8)$$

This is the margin between ID and OOD ranking scores. The logistic term $\log(1 + \exp(-\beta \Delta E_\phi))$ is small when the ordering is correct with an appropriate gap, large when the pair is misranked, and steepest near the decision boundary. Thus, the loss translates AUROC’s ranking objective into gradient updates that concentrate on pairs misordered or close to being misordered. To formalize this intuition, we examine the gradient and find it naturally emphasizes misranked or borderline pairs. Additional gradient and curvature derivations are provided in Appendix A.2.

Proposition 4.1 (Hard-pair emphasis). Let $d_\phi = \nabla_\phi E_\phi(S_{\text{out}}) - \nabla_\phi E_\phi(S_{\text{in}})$. A gradient step of size $\eta > 0$ on Eq. 6 changes the margin by

$$\delta(\Delta E_\phi) \approx \eta \beta \sigma(-\beta \Delta E_\phi) \|d_\phi\|_2^2 \geq 0, \quad (9)$$

where $\sigma(u) = (1 + e^{-u})^{-1}$. The weight $\sigma(-\beta \Delta E_\phi)$ decreases with ΔE_ϕ , which means it is largest for misranked or borderline pairs and smallest for already separated pairs. The detailed proof is provided in Appendix A.3 and additional experiments are provided in Appendix C.

Proposition 4.1 reveals the intuition behind Mole-PAIR. During training, the model naturally focuses more on the pairs that degrade AUROC the most—those that are misranked or near the boundary. These pairs receive stronger gradient updates, enlarging their margins first and further separating ID from OOD samples. Thus, the dynamics are self-correcting: once a pair is confidently ranked, it no longer consumes optimization effort, and the model shifts attention to the remaining hard cases. This aligns with the nature of AUROC, which is only affected by misranked or borderline pairs, and ensures that training resources are allocated to the most critical regions of the score distribution. For further practical details on the gradient behavior, see Appendix A.7.

4.2 CONVERGENCE TO THE OPTIMAL RANKING

The analysis above explains how our training objective dynamically prioritizes difficult pairs. We now demonstrate that this process converges to a globally optimal solution. We will prove that, given sufficient data and model capacity, the learned scorer achieves the Bayes-optimal ranking.

We define an ID-preference score:

$$f(S) \triangleq -E_\phi(S), \quad (10)$$

so that larger f means “more ID-like” (equivalently, lower ranking score). For any two samples S, S' , the pairwise score margin is:

$$z(S, S') \triangleq f(S) - f(S') = E_\phi(S') - E_\phi(S). \quad (11)$$

Thus $z > 0$ means that S is ranked ahead of S' as ID (i.e., $E_\phi(S) < E_\phi(S')$).

Lemma 4.2 (Local Pairwise Optimality). Let $\eta(S) = \Pr(\text{ID} \mid S)$ be the true posterior probability that a sample S is in-distribution. For any two samples S, S' , consider the conditional pairwise risk for $z = f(S) - f(S')$:

$$r_\beta(z; S, S') = \eta(S)(1 - \eta(S')) \log(1 + e^{-\beta z}) + \eta(S')(1 - \eta(S)) \log(1 + e^{\beta z}). \quad (12)$$

Then $r_\beta(z; S, S')$ is strictly convex in z and is minimized at:

$$z^* = \beta^{-1} \log \frac{\eta(S)[1 - \eta(S')]}{\eta(S')[1 - \eta(S)]}, \quad (13)$$

whose sign matches that of $\eta(S) - \eta(S')$. The detailed proof is provided in Appendix A.4.

Lemma 4.2 shows that for any pair (S, S') , the optimal score margin z^* aligns perfectly with the true posterior probabilities. If S is more likely to be ID than S' (i.e., $\eta(S) > \eta(S')$), the optimal margin z^* is positive, correctly ranking S higher. If both are equally likely, the optimal margin is zero, ensuring the model does not impose an artificial preference on an ambiguous pair. Furthermore, the magnitude of this optimal gap, $|z^*|$, scales with the confidence in the ordering (i.e., the distance between posteriors), while the temperature β simply rescales this gap without altering the ranking.

Proposition 4.3 (Global Convergence to the Bayes-Optimal Ranking). Define the pairwise risk of a scorer f by:

$$\mathcal{R}_\beta(f) = \mathbb{E}_{(S_{\text{in}}, S_{\text{out}})} \left[\log \left(1 + e^{-\beta [f(S_{\text{in}}) - f(S_{\text{out}})]} \right) \right], \quad (14)$$

where the expectation is over independent draws $S_{\text{in}} \sim D_{\text{in}}$ and $S_{\text{out}} \sim D_{\text{out}}$. For any sufficiently expressive function class, every global minimizer f^* of \mathcal{R}_β induces the same ordering as $\eta(\cdot)$ for almost all pairs, and hence achieves the Bayes-optimal AUROC (Detailed proof in Appendix A.5).

Lemma 4.2 establishes the optimal behavior for a single pair of samples, while Proposition 4.3 generalizes this local result to the entire data distribution. The proposition asserts that optimizing the global risk—an expectation over all ID-OOD pairs—drives the scorer towards the Bayes-optimal

ranking. Since the global objective is an aggregate of these pairwise terms, any scorer that systematically misranks a set of pairs can be improved by adjusting its scores towards the local optima defined in Lemma 4.2. Therefore, with sufficient model capacity and data, minimizing our pairwise objective recovers the true ranking induced by $\eta(\cdot)$, which by definition maximizes the AUROC. For the $\beta \rightarrow \infty$ asymptotics and the link to 0–1 ranking, see Appendix A.6.

5 EXPERIMENTS

Mole-PAIR can be applied to OOD detection across diverse tasks as a single model. In this section, we present empirical evidence to validate the effectiveness of the Mole-PAIR framework. The goal of our experiments is to demonstrate the practical efficacy of our approach in enhancing the OOD detection capabilities of existing molecular foundation models, rather than outperforming state-of-the-art methods specifically tailored for molecular OOD detection.

Datasets. With increasing attention on molecular OOD detection, two key benchmarks have been proposed: DrugOOD (Ji et al., 2022) and GOOD (Gui et al., 2022). DrugOOD is a systematic OOD dataset curator and benchmark for drug discovery, offering large-scale, realistic, and diverse datasets. To cover a variety of shifts that naturally occur in molecules, we cautiously selected three properties to divide the ID and OOD data: assay, molecular size, and molecular scaffold, respectively. GOOD is another systematic OOD benchmark that provides carefully designed data environments for distribution shifts. From this benchmark, we mainly consider covariate shift in our experiments.

Evaluation Metrics. In the experiments, we mainly report the following metrics: (1) the area under the receiver operating characteristic curve (AUROC), (2) the area under the precision-recall curve (AUPR), and (3) the false positive rate FPR95 of OOD samples when the true positive rate of ID samples is 95%. More baseline details can be found in Appendix B.2.

Training Details. We use pretrained MiniMol (Kläser et al., 2024) (2D graph features) and Uni-Mol (Zhou et al., 2023; Lu et al., 2024) (3D conformational features) as frozen encoders, each yielding a fixed 512-dimensional representation per molecule. Our Mole-PAIR module attaches a lightweight MLP scoring head with structure $512 \rightarrow 256 \rightarrow 128 \rightarrow 1$ and dropout 0.1; this head is the only trainable part. Mole-PAIR is trained without class labels, using only ID/OOD pairing signals. We optimize with AdamW (learning rate 1×10^{-4} , weight decay 1×10^{-5}), apply a StepLR scheduler (step size 10, $\gamma = 0.9$), and clip gradients at norm 1.0. The temperature is $\beta = 0.1$. Training runs for up to 500 epochs with batch size 512 for MiniMol and 256 for Uni-mol; inference uses the corresponding encoder-specific batch sizes.

Baselines. For supervised baselines we attach a classifier head to the same frozen 512-dimensional features. The head is an MLP with three layers and the hidden dimension is set to 64. The loss is CrossEntropyLoss for single-task classification, BCEWithLogitsLoss for multi-task classification, and MSELoss for regression when present prior to binarization. For datasets with continuous targets such as GOOD-ZINC, we binarize by a median split (label 1 if the value is \geq median, else 0) and train the classifier accordingly. Optimization uses Adam with learning rate 0.01 and weight decay 5×10^{-4} for 500 epochs, with early stopping (patience = 30) and best-validation checkpointing. To ensure fairness, when baselines are evaluated together we reuse the same trained checkpoint for scoring; when trained separately, each baseline uses the same architecture, hyperparameters, and splits. Based on this backbone, OOD scores are computed using MSP (Hendrycks & Gimpel, 2016), ODIN (Liang et al., 2017), Energy (Liu et al., 2020), Mahalanobis (Lee et al., 2018), LOF (Breunig et al., 2000), and KNN (Sun et al., 2022) as defined in the baseline section.

5.1 OVERALL PERFORMANCE

Our experimental results, summarized for AUROC in Table 1 and FPR95 in Table 2, reveal a fundamental limitation of standard baselines for molecular out-of-distribution detection. For comprehensive results including AUPR, see Table 5 in Appendix C. Confidence-based approaches such as MSP and ODIN consistently underperform under realistic distribution shifts. For example, on the MiniMol-EC50-Scaffold split, MSP yields an AUROC of 0.677 with an FPR95 of 0.725, and performance further deteriorates on the HIV-Scaffold split with an AUROC of 0.408 and an FPR95 of

Table 1: Out-of-distribution detection results measured by **AUROC** (\uparrow). The best results of all methods are indicated in boldface, and the second best results are underlined.

EC50			IC50			HIV		PCBA		ZINC	
Scaffold	Size	Assay	Scaffold	Size	Assay	Scaffold	Size	Scaffold	Size	Scaffold	Size
MiniMol											
MSP	0.677	0.449	0.420	0.574	0.515	0.600	0.408	0.194	0.632	0.697	0.359
ODIN	0.633	0.450	0.437	0.575	0.516	<u>0.614</u>	0.390	0.336	0.623	0.691	0.360
Energy	<u>0.685</u>	0.527	0.455	0.562	0.573	0.569	0.388	0.167	<u>0.642</u>	<u>0.735</u>	0.359
Mahalanobis	0.660	0.831	<u>0.572</u>	0.620	0.751	0.516	0.503	0.918	0.564	0.728	<u>0.638</u>
LOF	0.665	0.838	0.537	0.625	0.745	0.564	0.508	0.889	0.564	0.687	0.544
KNN	0.671	0.855	0.569	0.655	0.765	0.502	0.562	0.921	0.459	0.527	0.636
Mole-PAIR	0.970	1.000	0.711	0.983	0.999	0.660	0.777	1.000	0.924	1.000	0.614
<i>Improvement</i>	$\uparrow 41.6\%$	$\uparrow 17.0\%$	$\uparrow 24.3\%$	$\uparrow 50.1\%$	$\uparrow 30.6\%$	$\uparrow 7.5\%$	$\uparrow 38.3\%$	$\uparrow 8.6\%$	$\uparrow 43.9\%$	$\uparrow 36.1\%$	$\downarrow -3.76\%$
Unimol											
MSP	0.694	0.722	0.547	0.585	0.637	0.549	0.465	0.218	0.476	0.350	0.352
ODIN	0.621	0.656	0.558	0.546	0.591	0.538	0.451	0.278	0.445	0.353	0.352
Energy	0.691	0.652	0.547	0.542	0.598	0.551	0.476	0.243	0.476	0.350	0.369
Mahalanobis	0.724	0.784	0.591	0.699	0.723	0.562	0.567	0.826	0.568	0.690	<u>0.643</u>
LOF	<u>0.748</u>	<u>0.855</u>	0.558	<u>0.717</u>	<u>0.759</u>	0.547	<u>0.594</u>	<u>0.860</u>	0.538	0.607	0.577
KNN	0.704	0.747	<u>0.599</u>	0.682	0.660	<u>0.575</u>	0.580	0.826	0.553	0.668	<u>0.645</u>
Mole-PAIR	0.965	1.000	0.650	0.977	1.000	0.640	0.728	1.000	0.875	1.000	0.549
<i>Improvement</i>	$\uparrow 29.0\%$	$\uparrow 17.0\%$	$\uparrow 8.5\%$	$\uparrow 36.3\%$	$\uparrow 31.8\%$	$\uparrow 11.3\%$	$\uparrow 22.6\%$	$\uparrow 16.3\%$	$\uparrow 54.1\%$	$\uparrow 44.9\%$	$\downarrow -14.9\%$

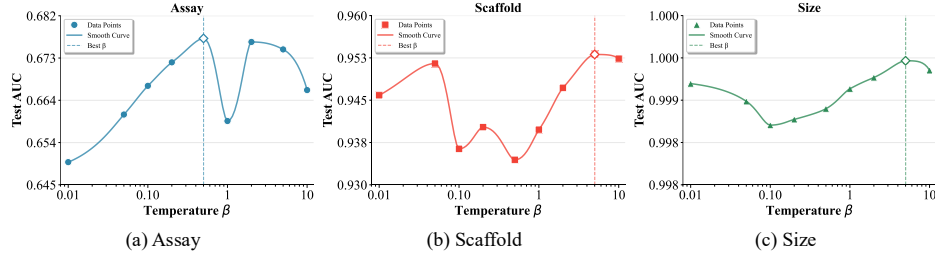


Figure 3: **Test AUROC sensitivity to the temperature β with $\lambda = 0.01$.** Different distribution shifts show distinct sensitivities: **Assay** prefers a medium β , **Scaffold** favors a larger β , while **Size** is largely insensitive to the choice of β .

0.953, where the model assigns high confidence to almost all novel OOD molecules. More advanced density- and distance-based methods offer occasional gains but remain unstable and unreliable.

In contrast, Mole-PAIR consistently surpasses all baselines across datasets, distribution shifts, and model backbones. On MiniMol–EC50–Scaffold, Mole-PAIR raises the AUROC from 0.677 to 0.970 and reduces the FPR95 from 0.725 to 0.178. On size-based splits, it often achieves near-perfect results with AUROC close to 1.000 and FPR95 near 0.000. Even on the most challenging setting such as HIV–Scaffold, Mole-PAIR delivers substantial improvements. These gains hold for both the lightweight MiniMol and the powerful Unimol encoder, underscoring its broad applicability.

Overall, these findings demonstrate that Mole-PAIR directly addresses the central challenge of molecular OOD detection, namely chemical hallucination. By optimizing the relative ranking between ID and OOD samples rather than relying on absolute confidence scores, it effectively reduces false positives, for instance lowering FPR95 from above 0.90 to below 0.20 on assay splits. As a lightweight, label-free, and backbone-agnostic framework, Mole-PAIR transforms molecular foundation models into reliable and robust tools for high-stakes applications such as drug discovery.

5.2 ABLATION STUDIES

The effect of temperature parameter β . We conduct experiments over various β in Eq. 6 while keeping the ℓ_2 regularization λ fixed at 0.01, and the experimental results are shown in Figure 3. Specifically, we list the test AUC performance with different values of β ranging from 0.01 to 10.0 on the EC50 dataset, under the Scaffold, Size, and Assay distribution shifts. From the figure, we find that different distribution shifts exhibit distinct sensitivities to the choice of β . The performance on the Scaffold split is highly sensitive to β , showing a non-monotonic trend where the optimal performance ($AUC \approx 0.953$) is achieved at a relatively large value ($\beta=5.0$). In contrast, the performance

Table 2: Comparison of OOD detection performance in terms of FPR95 (\downarrow). Lower values indicate better detection performance. Results are reported across different datasets and distribution shifts. Best results are in **bold**, and second-best are underlined.

	EC50			IC50			HIV		PCBA		ZINC	
	Scaffold	Size	Assay	Scaffold	Size	Assay	Scaffold	Size	Scaffold	Size	Scaffold	Size
MiniMol												
MSP	0.725	0.833	0.972	0.759	0.743	0.903	0.953	0.983	0.833	0.698	0.985	0.946
ODIN	0.734	0.832	0.950	<u>0.563</u>	0.741	<u>0.900</u>	0.962	0.819	0.856	0.763	0.985	0.947
Energy	<u>0.716</u>	0.726	0.973	0.781	<u>0.662</u>	0.905	0.955	0.985	<u>0.832</u>	0.697	0.985	0.946
Mahalanobis	0.898	<u>0.633</u>	<u>0.929</u>	0.909	0.786	0.946	0.947	<u>0.315</u>	0.922	0.752	0.905	0.874
LOF	0.893	0.667	0.933	0.909	0.803	0.934	0.943	0.458	0.934	0.804	0.933	<u>0.797</u>
KNN	0.870	0.550	0.930	0.898	0.782	0.942	<u>0.906</u>	0.280	0.960	0.902	0.906	0.801
Mole-PAIR	0.178	0.000	0.823	0.084	0.004	0.861	0.624	0.001	0.348	0.001	<u>0.925</u>	0.000
<i>Improvement</i>	$\uparrow 75.4\%$	$\uparrow 100.0\%$	$\uparrow 11.4\%$	$\uparrow 85.1\%$	$\uparrow 99.4\%$	$\uparrow 4.3\%$	$\uparrow 31.1\%$	$\uparrow 99.7\%$	$\uparrow 58.2\%$	$\uparrow 99.9\%$	$\downarrow -2.21\%$	$\uparrow 100.0\%$
Unimol												
MSP	0.848	0.733	0.957	0.926	0.861	0.945	0.954	0.985	0.954	0.925	0.992	0.996
ODIN	<u>0.816</u>	0.798	<u>0.913</u>	0.945	0.911	0.943	0.947	0.977	0.962	0.925	0.993	0.997
Energy	0.849	0.740	0.948	0.935	0.872	0.949	0.952	0.982	0.954	0.925	0.993	0.996
Mahalanobis	0.831	0.605	0.921	<u>0.818</u>	<u>0.718</u>	0.936	0.920	<u>0.514</u>	<u>0.836</u>	<u>0.855</u>	0.965	0.938
LOF	0.844	<u>0.554</u>	0.935	0.832	0.746	0.942	0.894	0.567	0.948	0.926	0.945	0.919
KNN	0.855	0.707	0.914	0.833	0.806	<u>0.929</u>	<u>0.885</u>	0.563	0.941	0.895	0.961	<u>0.899</u>
Mole-PAIR	0.178	0.000	0.869	0.139	0.000	0.890	0.736	0.000	0.515	0.000	<u>0.949</u>	0.000
<i>Improvement</i>	$\uparrow 78.2\%$	$\uparrow 100\%$	$\uparrow 4.8\%$	$\uparrow 83.1\%$	$\uparrow 100\%$	$\uparrow 4.2\%$	$\uparrow 16.8\%$	$\uparrow 100\%$	$\uparrow 38.4\%$	$\uparrow 100\%$	$\downarrow -0.42\%$	$\uparrow 100\%$

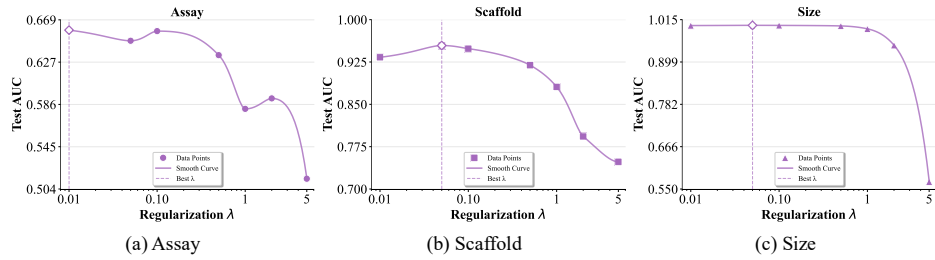


Figure 4: **Test AUROC sensitivity to the ℓ_2 regularization λ with $\beta = 0.1$.** Performance varies with regularization strength: **Assay** performs best with weak regularization, **Scaffold** benefits from a modest amount of regularization, while **Size** is robust until the regularization becomes too strong.

on the Size split is robust and largely insensitive to β , achieving near-perfect AUC scores across the entire range of values. The performance on the Assay split also shows moderate sensitivity, peaking at $\beta=0.5$. This not only demonstrates the effectiveness of our Mole-PAIR framework but also reveals that complex shifts, like scaffold difference, are harder to learn and benefit from a stronger preference optimization signal, whereas simpler shifts based on molecular size are easily separable regardless of the signal strength.

The influence of regularization parameter λ . We further analyze the effect of the regularization coefficient λ while keeping the DPO temperature β fixed at 0.1. The results across the three distribution shifts on the EC50 dataset are shown in Figure 4. The datasets demonstrate varied sensitivities to λ . For the Assay split, performance is optimal with a small regularization ($\lambda \leq 0.1$) and degrades steadily as the penalty increases. The Scaffold split exhibits a clearer trend, with performance peaking at an optimal value of $\lambda=0.05$ before declining sharply, indicating that a modest amount of regularization is beneficial for this complex task. Conversely, the Size split is robust to a wide range of regularization strengths, maintaining near-perfect performance for λ up to 1.0, after which it drops precipitously. Overall, these findings highlight the role of λ as a critical hyperparameter. While an optimal value can improve generalization on challenging shifts like Scaffold, an excessively large regularization coefficient is consistently detrimental to performance across all tasks, likely due to over-constraining the ranking function and preventing effective separation.

6 CONCLUSION

In this paper, we propose Mole-PAIR, a lightweight, plug-and-play, and model-agnostic framework that can be flexibly integrated with existing foundation models to endow them with OOD detection capabilities. Unlike conventional approaches which resort to point-wise estimation and optimization, we innovatively reframe the OOD detection problem as a preference optimization problem by carefully devising a pairwise loss. We theoretically justify that this pairwise learning objective aligns with the AUROC metric, which measures how consistently the model ranks ID samples higher than OOD samples. Extensive experiments on five real-world datasets under three different kinds of distribution shifts demonstrate the effectiveness and superiority of our model.

REFERENCES

Anastasios N Angelopoulos, Stephen Bates, Adam Fisch, Lihua Lei, and Tal Schuster. Conformal risk control. *arXiv preprint arXiv:2208.02814*, 2022.

Staffan Arvidsson McShane, Ulf Norinder, Jonathan Alvarsson, Ernst Ahlberg, Lars Carlsson, and Ola Spjuth. Cpsign: conformal prediction for cheminformatics modeling. *Journal of Cheminformatics*, 16(1):75, 2024.

Tianyi Bao, Qitian Wu, Zetian Jiang, Yiting Chen, Jiawei Sun, and Junchi Yan. Graph out-of-distribution detection goes neighborhood shaping. In *Forty-first International Conference on Machine Learning*, 2024.

Dominique Beaini, Shenyang Huang, Joao Alex Cunha, Zhiyi Li, Gabriela Moisescu-Pareja, Oleksandr Dymov, Samuel Maddrell-Mander, Callum McLean, Frederik Wenkel, Luis Müller, et al. Towards foundational models for molecular learning on large-scale multi-task datasets. *arXiv preprint arXiv:2310.04292*, 2023.

Ralph Allan Bradley and Milton E Terry. Rank analysis of incomplete block designs: I. the method of paired comparisons. *Biometrika*, 39(3/4):324–345, 1952.

Markus M Breunig, Hans-Peter Kriegel, Raymond T Ng, and Jörg Sander. Lof: identifying density-based local outliers. In *Proceedings of the 2000 ACM SIGMOD international conference on Management of data*, pp. 93–104, 2000.

Corinna Cortes and Mehryar Mohri. Auc optimization vs. error rate minimization. *Advances in neural information processing systems*, 16, 2003.

Laurianne David, Amol Thakkar, Rocío Mercado, and Ola Engkvist. Molecular representations in ai-driven drug discovery: a review and practical guide. *Journal of cheminformatics*, 12(1):56, 2020.

Xuefeng Du, Yiyu Sun, Xiaojin Zhu, and Yixuan Li. Dream the impossible: Outlier imagination with diffusion models, 2023. URL <https://arxiv.org/abs/2309.13415>.

Tom Fawcett. An introduction to roc analysis. *Pattern recognition letters*, 27(8):861–874, 2006.

Yonatan Geifman and Ran El-Yaniv. Selective classification for deep neural networks. *Advances in neural information processing systems*, 30, 2017.

Yonatan Geifman and Ran El-Yaniv. Selectivenet: A deep neural network with an integrated reject option. In *International conference on machine learning*, pp. 2151–2159. PMLR, 2019.

Shurui Gui, Xiner Li, Limei Wang, and Shuiwang Ji. Good: A graph out-of-distribution benchmark, 2022. URL <https://arxiv.org/abs/2206.08452>.

Chuan Guo, Geoff Pleiss, Yu Sun, and Kilian Q Weinberger. On calibration of modern neural networks. In *International conference on machine learning*, pp. 1321–1330. PMLR, 2017.

Yuxin Guo, Cheng Yang, Yuluo Chen, Jixi Liu, Chuan Shi, and Junping Du. A data-centric framework to endow graph neural networks with out-of-distribution detection ability. In *Proceedings of the 29th ACM SIGKDD conference on knowledge discovery and data mining*, pp. 638–648, 2023.

Dan Hendrycks and Kevin Gimpel. A baseline for detecting misclassified and out-of-distribution examples in neural networks. *arXiv preprint arXiv:1610.02136*, 2016.

Jiwoo Hong, Noah Lee, and James Thorne. Orpo: Monolithic preference optimization without reference model. *arXiv preprint arXiv:2403.07691*, 2024.

Yuanfeng Ji, Lu Zhang, Jiaxiang Wu, Bingzhe Wu, Long-Kai Huang, Tingyang Xu, Yu Rong, Lanqing Li, Jie Ren, Ding Xue, Houtim Lai, Shaoyong Xu, Jing Feng, Wei Liu, Ping Luo, Shuigeng Zhou, Junzhou Huang, Peilin Zhao, and Yatao Bian. Drugood: Out-of-distribution (ood) dataset curator and benchmark for ai-aided drug discovery – a focus on affinity prediction problems with noise annotations, 2022. URL <https://arxiv.org/abs/2201.09637>.

Shengli Jiang, Shiyi Qin, Reid C Van Lehn, Prasanna Balaprakash, and Victor M Zavala. Uncertainty quantification for molecular property predictions with graph neural architecture search. *Digital Discovery*, 3(8):1534–1553, 2024.

Thorsten Joachims. Optimizing search engines using clickthrough data. In *Proceedings of the eighth ACM SIGKDD international conference on Knowledge discovery and data mining*, pp. 133–142, 2002.

Kerstin Kläser, Błażej Banaszewski, Samuel Maddrell-Mander, Callum McLean, Luis Müller, Ali Parviz, Shenyang Huang, and Andrew Fitzgibbon. MiniMol: A parameter-efficient foundation model for molecular learning, 2024. URL <https://arxiv.org/abs/2404.14986>.

Siddhartha Laghuvarapu, Zhen Lin, and Jimeng Sun. Codrug: Conformal drug property prediction with density estimation under covariate shift. *Advances in Neural Information Processing Systems*, 36:37728–37747, 2023.

Kimin Lee, Kibok Lee, Honglak Lee, and Jinwoo Shin. A simple unified framework for detecting out-of-distribution samples and adversarial attacks. *Advances in neural information processing systems*, 31, 2018.

Jing Lei, Max G’Sell, Alessandro Rinaldo, Ryan J Tibshirani, and Larry Wasserman. Distribution-free predictive inference for regression. *Journal of the American Statistical Association*, 113(523):1094–1111, 2018.

Yucen Lily Li, Daohan Lu, Polina Kirichenko, Shikai Qiu, Tim G. J. Rudner, C. Bayan Bruss, and Andrew Gordon Wilson. Out-of-distribution detection methods answer the wrong questions, 2025. URL <https://arxiv.org/abs/2507.01831>.

Zenan Li, Qitian Wu, Fan Nie, and Junchi Yan. Graphde: A generative framework for debiased learning and out-of-distribution detection on graphs. *Advances in Neural Information Processing Systems*, 35:30277–30290, 2022.

Shiyu Liang, Yixuan Li, and Rayadurgam Srikant. Enhancing the reliability of out-of-distribution image detection in neural networks. *arXiv preprint arXiv:1706.02690*, 2017.

Zeming Lin, Halil Akin, Roshan Rao, Brian Hie, Zhongkai Zhu, Wenting Lu, Nikita Smetanin, Robert Verkuil, Ori Kabeli, Yaniv Shmueli, et al. Evolutionary-scale prediction of atomic-level protein structure with a language model. *Science*, 379(6637):1123–1130, 2023.

Fei Tony Liu, Kai Ming Ting, and Zhi-Hua Zhou. Isolation forest. In *2008 eighth ieee international conference on data mining*, pp. 413–422. IEEE, 2008.

Weitang Liu, Xiaoyun Wang, John Owens, and Yixuan Li. Energy-based out-of-distribution detection. *Advances in neural information processing systems*, 33:21464–21475, 2020.

Yixin Liu, Kaize Ding, Huan Liu, and Shirui Pan. Good-d: On unsupervised graph out-of-distribution detection. In *Proceedings of the sixteenth ACM international conference on web search and data mining*, pp. 339–347, 2023.

Shuqi Lu, Zhifeng Gao, Di He, Linfeng Zhang, and Guolin Ke. Data-driven quantum chemical property prediction leveraging 3d conformations with uni-mol+. *Nature Communications*, 15(1):7104, 2024.

Yizhen Luo, Kai Yang, Massimo Hong, Xing Yi Liu, and Zaiqing Nie. Molfm: A multimodal molecular foundation model. *arXiv preprint arXiv:2307.09484*, 2023.

Gerald M. Maggiora. On outliers and activity cliffswwhy qsar often disappoints. *Journal of Chemical Information and Modeling*, 46(4):1535–1535, 2006. doi: 10.1021/ci060117s. URL <https://doi.org/10.1021/ci060117s>. PMID: 16859285.

Oscar Méndez-Lucio, Christos A Nicolaou, and Berton Earnshaw. Mole: a foundation model for molecular graphs using disentangled attention. *Nature Communications*, 15(1):9431, 2024.

Yu Meng, Mengzhou Xia, and Danqi Chen. Simpo: Simple preference optimization with a reference-free reward. *Advances in Neural Information Processing Systems*, 37:124198–124235, 2024.

Rafael Rafailov, Archit Sharma, Eric Mitchell, Stefano Ermon, Christopher D. Manning, and Chelsea Finn. Direct preference optimization: Your language model is secretly a reward model, 2024. URL <https://arxiv.org/abs/2305.18290>.

Bharath Ramsundar, Bowen Liu, Zhenqin Wu, Andreas Verras, Matthew Tudor, Robert P. Sheridan, and Vijay Pande. Is multitask deep learning practical for pharma? *Journal of Chemical Information and Modeling*, 57(8):2068–2076, 2017. doi: 10.1021/acs.jcim.7b00146. URL <https://doi.org/10.1021/acs.jcim.7b00146>. PMID: 28692267.

Yaniv Romano, Matteo Sesia, and Emmanuel Candes. Classification with valid and adaptive coverage. *Advances in neural information processing systems*, 33:3581–3591, 2020.

Yu Rong, Yatao Bian, Tingyang Xu, Weiyang Xie, Ying Wei, Wenbing Huang, and Junzhou Huang. Self-supervised graph transformer on large-scale molecular data. *Advances in neural information processing systems*, 33:12559–12571, 2020.

Benjamin Sanchez-Lengeling, Carlos Outeiral, Gabriel L Guimaraes, and Alan Aspuru-Guzik. Optimizing distributions over molecular space. an objective-reinforced generative adversarial network for inverse-design chemistry (organic). *ACS Central Science*, 2017.

Bernhard Schölkopf, Robert C Williamson, Alex Smola, John Shawe-Taylor, and John Platt. Support vector method for novelty detection. *Advances in neural information processing systems*, 12, 1999.

Xu Shen, Yili Wang, Kaixiong Zhou, Shirui Pan, and Xin Wang. Optimizing ood detection in molecular graphs: A novel approach with diffusion models, 2024. URL <https://arxiv.org/abs/2404.15625>.

Yiyou Sun, Yifei Ming, Xiaojin Zhu, and Yixuan Li. Out-of-distribution detection with deep nearest neighbors. In *International conference on machine learning*, pp. 20827–20840. PMLR, 2022.

Lewis Tunstall, Edward Beeching, Nathan Lambert, Nazneen Rajani, Kashif Rasul, Younes Belkada, Shengyi Huang, Leandro Von Werra, Clémentine Fourrier, Nathan Habib, et al. Zephyr: Direct distillation of lm alignment. *arXiv preprint arXiv:2310.16944*, 2023.

Derek van Tilborg, Alisa Alenicheva, and Francesca Grisoni. Exposing the limitations of molecular machine learning with activity cliffs. *Journal of Chemical Information and Modeling*, 62(23): 5938–5951, 2022. doi: 10.1021/acs.jcim.2c01073. URL <https://doi.org/10.1021/acs.jcim.2c01073>. PMID: 36456532.

Chaoqi Wang, Yibo Jiang, Chenghao Yang, Han Liu, and Yuxin Chen. Beyond reverse kl: Generalizing direct preference optimization with diverse divergence constraints. *arXiv preprint arXiv:2309.16240*, 2023.

Danny Wang, Ruihong Qiu, Guangdong Bai, and Zi Huang. Gold: Graph out-of-distribution detection via implicit adversarial latent generation. *arXiv preprint arXiv:2502.05780*, 2025a.

Fangxin Wang, Yuqing Liu, Kay Liu, Yibo Wang, Sourav Medya, and Philip S Yu. Uncertainty in graph neural networks: A survey. *arXiv preprint arXiv:2403.07185*, 2024.

Fangxin Wang, Yuqing Liu, Kay Liu, Yibo Wang, Sourav Medya, and Philip S. Yu. Uncertainty in graph neural networks: A survey, 2025b. URL <https://arxiv.org/abs/2403.07185>.

Qitian Wu, Yiting Chen, Chenxiao Yang, and Junchi Yan. Energy-based out-of-distribution detection for graph neural networks. *arXiv preprint arXiv:2302.02914*, 2023.

Shirley Wu, Kaidi Cao, Bruno Ribeiro, James Zou, and Jure Leskovec. Graphmetro: Mitigating complex graph distribution shifts via mixture of aligned experts, 2024. URL <https://arxiv.org/abs/2312.04693>.

Ziwei Xu, Sanjay Jain, and Mohan Kankanhalli. Hallucination is inevitable: An innate limitation of large language models, 2025. URL <https://arxiv.org/abs/2401.11817>.

Gengmo Zhou, Zhifeng Gao, Qiankun Ding, Hang Zheng, Hongteng Xu, Zhewei Wei, Linfeng Zhang, and Guolin Ke. Uni-mol: A universal 3d molecular representation learning framework. In *The Eleventh International Conference on Learning Representations*, 2023. URL <https://openreview.net/forum?id=6K2RM6wVqKu>.

Junyou Zhu, Langzhou He, Chao Gao, Dongpeng Hou, Zhen Su, Philip S Yu, Juergen Kurths, and Frank Hellmann. Sdmg: Smoothing your diffusion models for powerful graph representation learning. In *Proceedings of the 42nd International Conference on Machine Learning*, 2025.

A DERIVATION AND PROOF

A.1 NOTATION AND SETUP

Let $E_\phi : \mathcal{X} \rightarrow \mathbb{R}$ be a differentiable scoring head with parameters ϕ (the encoder is frozen). For any ID–OOD pair $(S_{\text{in}}, S_{\text{out}})$ we define the margin

$$\Delta E_\phi \triangleq E_\phi(S_{\text{out}}) - E_\phi(S_{\text{in}}), \quad (15)$$

which is identical to Eq. 8 in the main text. The per-pair logistic term is

$$\ell(\Delta E_\phi) = \log(1 + \exp(-\beta \Delta E_\phi)), \quad (16)$$

and the objective is the pairwise expectation

$$\mathcal{L}(\phi) = \mathbb{E}_{S_{\text{in}} \sim D_{\text{in}}, S_{\text{out}} \sim D_{\text{out}}} [\ell(\Delta E_\phi)], \quad (17)$$

which coincides with Eq. 6 (and its expectation form Eq. 14 after the change $f = -E_\phi$ used in the main text). When needed, we also consider the total objective with a small ℓ_2 gauge-fixing term

$$\mathcal{L}_{\text{tot}}(\phi) = \mathcal{L}(\phi) + \frac{\lambda}{2} \mathbb{E}_{S \sim \Pi} [E_\phi(S)^2], \quad (18)$$

matching Eq. 7 in the main text; here Π is any fixed sampling measure on \mathcal{X} (e.g., the mixture of D_{in} and D_{out}).

A.2 FULL GRADIENT AND CURVATURE CALCULATIONS

Gradient w.r.t. the margin. For $z = \Delta E_\phi$ we have

$$\begin{aligned} \ell'(z) &= \frac{\partial}{\partial z} \log(1 + e^{-\beta z}) = -\frac{\beta}{1 + e^{\beta z}} = -\beta \sigma(-\beta z), \\ \ell''(z) &= \frac{\partial}{\partial z} \ell'(z) = \beta^2 \sigma(\beta z) \sigma(-\beta z) > 0, \end{aligned}$$

so ℓ is strictly convex in z .

Gradient w.r.t. parameters. By chain rule,

$$\begin{aligned} \nabla_\phi \ell(\Delta E_\phi) &= \ell'(\Delta E_\phi) \nabla_\phi \Delta E_\phi \\ &= -\beta \sigma(-\beta \Delta E_\phi) (\nabla_\phi E_\phi(S_{\text{out}}) - \nabla_\phi E_\phi(S_{\text{in}})). \end{aligned} \quad (19)$$

Define the direction term

$$d_\phi \triangleq \nabla_\phi E_\phi(S_{\text{out}}) - \nabla_\phi E_\phi(S_{\text{in}}),$$

and the weight function

$$w_\beta(t) \triangleq \beta \sigma(-\beta t) \in (0, \beta). \quad (20)$$

Then $\nabla_\phi \ell(\Delta E_\phi) = -w_\beta(\Delta E_\phi) d_\phi$ and

$$\nabla_\phi \mathcal{L}(\phi) = \mathbb{E}[-w_\beta(\Delta E_\phi) d_\phi].$$

Moreover,

$$w'_\beta(t) = -\beta^2 \sigma(\beta t) \sigma(-\beta t) < 0, \quad w_\beta(0) = \beta/2, \quad \lim_{t \rightarrow -\infty} w_\beta(t) = \beta, \quad \lim_{t \rightarrow +\infty} w_\beta(t) = 0,$$

so misranked ($t < 0$) or borderline ($t \approx 0$) pairs receive larger weights, while already-separated pairs ($t \gg 0$) are nearly ignored.

Per-example backprop signals. Differentiating Eq. 16 w.r.t. the scalar ranking score gives

$$\frac{\partial \ell}{\partial E_\phi(S_{\text{out}})} = -\beta \sigma(-\beta \Delta E_\phi), \quad \frac{\partial \ell}{\partial E_\phi(S_{\text{in}})} = +\beta \sigma(-\beta \Delta E_\phi),$$

equal in magnitude and opposite in sign. If E_ϕ is linear on a frozen representation $h(\cdot)$, i.e., $E_\phi(S) = \langle w, h(S) \rangle + b$, then d_ϕ reduces to $h(S_{\text{out}}) - h(S_{\text{in}})$ and the gradient is a simple contrastive update.

A.3 PROOF OF PROPOSITION 4.1

We show that a gradient step increases the margin by an amount proportional to $w_\beta(\Delta E_\phi) \|d_\phi\|_2^2$.

First-order calculation. A gradient descent step with stepsize $\eta > 0$ is

$$\phi^+ = \phi - \eta \nabla_\phi \ell(\Delta E_\phi) = \phi + \eta w_\beta(\Delta E_\phi) d_\phi.$$

By first-order Taylor expansion,

$$\begin{aligned} \delta(\Delta E_\phi) &\triangleq \Delta E_\phi(\phi^+) - \Delta E_\phi(\phi) \\ &\approx \nabla_\phi \Delta E_\phi(\phi)^\top (\phi^+ - \phi) \\ &= d_\phi^\top (\eta w_\beta(\Delta E_\phi) d_\phi) \\ &= \eta w_\beta(\Delta E_\phi) \|d_\phi\|_2^2 \\ &\geq 0. \end{aligned} \tag{21}$$

which yields Eq. 9 in the main text with $w_\beta(\cdot) = \beta \sigma(-\beta \cdot)$.

Second-order control (sufficient condition for strict increase). If $\nabla_\phi \Delta E_\phi$ is L -Lipschitz (equivalently, the Hessian of ΔE_ϕ has operator norm $\leq L$ on the segment between ϕ and ϕ^+), then Taylor's theorem gives

$$\delta(\Delta E_\phi) \geq \eta w_\beta(\Delta E_\phi) \|d_\phi\|_2^2 - \frac{L}{2} \|\eta w_\beta(\Delta E_\phi) d_\phi\|_2^2 = \eta w_\beta(\Delta E_\phi) \|d_\phi\|_2^2 \left(1 - \frac{L\eta}{2} w_\beta(\Delta E_\phi)\right).$$

Hence for any pair, choosing $\eta < 2/(L w_\beta(\Delta E_\phi))$ guarantees $\delta(\Delta E_\phi) > 0$.

A.4 PROOF OF LEMMA 4.2 (LOCAL PAIRWISE OPTIMALITY)

Define $f = -E_\phi$ so that larger f is “more ID-like”, as in the main text. For two samples S, S' let $z = f(S) - f(S') = E_\phi(S') - E_\phi(S)$ (Eq. 11). Let $\eta(S) = \Pr(\text{ID} \mid S)$ and set

$$\alpha \triangleq \eta(S)(1 - \eta(S')), \quad \alpha' \triangleq \eta(S')(1 - \eta(S)).$$

The conditional pairwise risk (Eq. 12) can be written

$$r_\beta(z; S, S') = \alpha \log(1 + e^{-\beta z}) + \alpha' \log(1 + e^{\beta z}).$$

Strict convexity. Using $\ell''(z) > 0$ from A.2, we have

$$\frac{\partial^2 r_\beta}{\partial z^2} = (\alpha + \alpha') \beta^2 \sigma(\beta z) \sigma(-\beta z) > 0 \quad \text{whenever } \alpha + \alpha' > 0,$$

so $r_\beta(z; S, S')$ is strictly convex in z for any non-degenerate pair.

Stationary point. Differentiating and setting to zero,

$$\frac{\partial r_\beta}{\partial z} = -\alpha \beta \sigma(-\beta z) + \alpha' \beta \sigma(\beta z) = 0 \iff \alpha \sigma(-\beta z) = \alpha' \sigma(\beta z).$$

Using $\sigma(\beta z)/\sigma(-\beta z) = e^{\beta z}$,

$$e^{\beta z^*} = \frac{\alpha}{\alpha'} = \frac{\eta(S)[1 - \eta(S')]}{\eta(S')[1 - \eta(S)]} \implies z^* = \frac{1}{\beta} \log \frac{\eta(S)[1 - \eta(S')]}{\eta(S')[1 - \eta(S)]},$$

which is Eq. 13. Since $u \mapsto \log(u/(1-u))$ is strictly increasing on $(0, 1)$, $\text{sign}(z^*) = \text{sign}(\eta(S) - \eta(S'))$.

A.5 PROOF OF PROPOSITION 4.3 (GLOBAL BAYES-OPTIMAL RANKING)

We now prove that, over a rich function class, any global minimizer of the population risk

$$\mathcal{R}_\beta(f) = \mathbb{E}_{(S_{\text{in}}, S_{\text{out}})} \left[\log \left(1 + e^{-\beta [f(S_{\text{in}}) - f(S_{\text{out}})]} \right) \right] \tag{Eq. 14}$$

induces the same ordering as $\eta(\cdot)$ for almost all pairs, hence achieves the Bayes-optimal AUROC.

A canonical minimizer realizing the point-wise optima simultaneously. Define

$$f^*(S) \triangleq \frac{1}{\beta} \log \frac{\eta(S)}{1 - \eta(S)} \quad (+ \text{ any additive constant}). \quad (22)$$

For any pair (S, S') , $z^* = f^*(S) - f^*(S')$ equals the two-point optimum from Lemma 4.2. Therefore, for every pair, $r_\beta(f^*(S) - f^*(S'); S, S')$ attains the *pairwise* minimal value. Integrating over pairs shows f^* minimizes the population risk \mathcal{R}_β . Moreover, if g is any other function with $\mathcal{R}_\beta(g) = \mathcal{R}_\beta(f^*)$, then for almost every pair (S, S') we must have $g(S) - g(S') = f^*(S) - f^*(S')$, hence $g - f^*$ is almost everywhere constant. Thus the set of global minimizers is exactly $\{f^* + c : c \in \mathbb{R}\}$. In particular, all global minimizers induce the same ordering as η .

Remarks. (i) Any strictly increasing transform $h \circ \eta$ induces the same ranking and hence achieves Bayes-optimal AUROC; however, it does not in general minimize \mathcal{R}_β unless $h(u) = \beta^{-1} \log(u/(1-u))$ up to an additive constant, because only then do all pairwise gaps equal z^* . (ii) The additive constant does not affect pairwise differences and hence leaves both AUROC and \mathcal{R}_β unchanged; the ℓ_2 term in Eq. 18 fixes this gauge without changing the induced ranking.

A.6 AUROC CONNECTION AND TEMPERATURE LIMIT

AUROC may be written as $\Pr(E_\phi(S_{\text{in}}) < E_\phi(S_{\text{out}}))$, i.e., the probability that ID ranks ahead of OOD (equivalently, $\Pr(\Delta E_\phi > 0)$), which is exactly the ranking event smoothed by $\ell(\cdot)$ in equation 16. As $\beta \rightarrow \infty$,

$$\ell(z) = \log(1 + e^{-\beta z}) \longrightarrow \begin{cases} 0, & z > 0, \\ \log 2, & z = 0, \\ +\infty, & z < 0, \end{cases}$$

so the function converges to a hard 0–1 ranking penalty that forbids misordered pairs ($z < 0$).

A.7 ADDITIONAL IMPLEMENTATION-FACING IDENTITIES

Steepness around the boundary. The magnitude of the per-pair backprop signal is

$$\|\nabla_\phi \ell(\Delta E_\phi)\| = w_\beta(\Delta E_\phi) \|d_\phi\| \leq \frac{\beta}{2} \|d_\phi\| \quad \text{with equality at } \Delta E_\phi = 0.$$

Hence updates concentrate near the decision boundary; the logistic slope is maximized at $\Delta E_\phi = 0$.

Invariance to shifts: role of ℓ_2 regularization. For any constant c , replacing E_ϕ by $E_\phi + c$ leaves ΔE_ϕ (and hence $\mathcal{L}(\phi)$ and AUROC) unchanged. The ℓ_2 term in Eq. 18 removes this degree of freedom by selecting the unique representative (up to sampling) with minimal squared energy norm, without affecting the ranking.

Effect of temperature β . Larger β sharpens $w_\beta(t)$ towards a hard 0–1 ranking loss, leading to faster correction of borderline pairs but potentially larger variance if margins become too large (gradient saturation for well-separated pairs). Smaller β smooths updates and can be numerically more forgiving; in all cases, Proposition 4.3 ensures the same Bayes-optimal ranking at the population optimum.

B EXPERIMENTS DETAILS

B.1 DATASET

DrugOOD Dataset. DrugOOD (Ji et al., 2022) is a benchmark and automated dataset curator for OOD challenges in AI-aided drug discovery, built from the large-scale ChEMBL bioassay database. It focuses on the crucial task of drug-target binding affinity prediction, which is framed as a binary classification problem (active vs. inactive). For this, we focus on the Ligand-Based Affinity Prediction (LBAP) variants of DrugOOD, which define three types of domain shifts based on biochemistry knowledge:

- **Assay:** Samples are split by the experimental assay, simulating shifts in experimental environments. Assays with many samples are used for training, while those with fewer are used for testing.
- **Scaffold:** Samples are split by their molecular scaffold structure. The largest scaffolds are assigned to the training set and the smallest to the test set to maximize structural diversity.
- **Size:** Samples are split by the number of atoms in the molecule. Molecules with the largest atomic sizes are used for training and smaller ones for testing to ensure variability.

Specifically, we use the `drugood_lbap_general_[ec50, ic50]_(assay, scaffold, size)` subsets, which are the standard LBAP partitions provided in DrugOOD. These subsets cover different types of domain shifts under both EC50 and IC50 measurement settings, offering diverse and challenging scenarios for OOD evaluation. Deterministic splits are constructed using `data_seed=42`, with the following target sizes: `train_id=2000`, `train_ood=2000`, `val_id=600`, `val_ood=600`, `test_id=1000`, and `test_ood=1000`. Supervised training labels are read from the `cls_label` field in the JSON files.

Table 3: List of used DrugOOD dataset. Pos and Neg denote the numbers of positive and negative data points, respectively. $D^{\#}$ represents the number of domains, and $C^{\#}$ represent the number of data points.

Data subset	Pos [#]	Neg [#]	Train		ID Val		ID Test		OOD Val		OOD Test	
			$D^{\#}$	$C^{\#}$								
drugood-lbap-core-ic50-assay	83802	11434	311	34179	311	11314	311	11683	314	19028	699	19032
drugood-lbap-core-ic50-scaffold	83802	11434	6881	21519	1912	4920	24112	30708	6345	19041	4350	19048
drugood-lbap-core-ic50-size	83802	11434	190	36597	140	12153	229	12411	4	17660	18	16415
drugood-lbap-core-ec50-assay	10199	2462	47	4540	47	1502	47	1557	46	2572	101	2490
drugood-lbap-core-ec50-scaffold	10200	2462	850	2570	224	580	3668	4447	1193	2532	953	2533
drugood-lbap-core-ec50-size	10200	2462	167	4684	103	1513	205	1753	4	2313	17	2399

GOOD Datasets. The GOOD (Gui et al., 2022) benchmark provides molecular graph datasets designed for systematic OOD evaluation. We use three datasets:

- **GOOD-HIV:** A small-scale dataset adapted from MoleculeNet. Inputs are molecular graphs with atoms as nodes and chemical bonds as edges. The task is binary classification to predict whether a molecule inhibits HIV replication.
- **GOOD-PCBA:** A large-scale dataset with 128 bioassays, forming a multi-target binary classification task.
- **GOOD-ZINC:** A molecular property regression dataset derived from the ZINC database, where molecules contain up to 38 heavy atoms. The task is to predict constrained solubility.

For our experiments, we generate deterministic splits with sizes: `train_id/train_ood=5000`, `val_id/val_ood=1500`, and `test_id/test_ood=2000`. Labels strictly follow the official benchmark protocol. For tasks that are regression-like, such as GOOD-ZINC, we binarize the target via a median split: samples with values greater than or equal to the median are assigned positive labels, and the rest are negative. This allows for the training of a supervised classifier, and OOD detection is then evaluated on the classifier’s outputs. Statistics of the datasets are summarized in Table 4.

Splitting, caching, and features. All dataset splits are generated deterministically using seed 42. We pre-compute molecular representations using foundation encoders and cache them for reuse. Feature extraction is performed with batch size 50, and the resulting representations are used both to train the supervised classifier head and as the basis for OOD scoring methods.

B.2 BASELINES

We compare against several widely used supervised OOD detection baselines, all of which operate on the logits or penultimate features of a trained classifier head. Unless otherwise specified, the OOD score is defined such that larger values indicate a higher likelihood of being out-of-distribution.

Dataset	Shift	Train	ID validation	ID test	OOD validation	OOD test	Train	OOD validation	ID validation	ID test	OOD test
		Scaffold				Size					
GOOD-HIV	covariate	24682	4112	4112	4113	4108	26169	4112	4112	2773	3961
	concept	15209	3258	3258	9365	10037	14454	3096	3096	9956	10525
	no shift	24676	8225	8226	-	-	24676	8225	8226	-	-
GOOD-PCBA	covariate	262764	43792	43792	44019	43562	269990	43792	43792	48430	31925
	concept	159158	34105	34105	90740	119821	150121	32168	32168	108267	115205
	no shift	262757	87586	87586	-	-	262757	87586	87586	-	-
GOOD-ZINC	covariate	149674	24945	24945	24945	24946	161893	24945	24945	20270	17402
	concept	101867	21828	21828	43539	60393	89418	19161	19161	51409	70306
	no shift	149673	49891	49891	-	-	149673	49891	49891	-	-

Table 4: Numbers of graphs in training, ID validation, ID test, OOD validation, and OOD test sets for the GOOD datasets.

MSP (Hendrycks & Gimpel, 2016) calculates the in-distribution (ID) score as the maximum class confidence from the classifier head’s logits. For multi-class tasks, this is the maximum softmax probability, while for binary or single-output tasks it is $\max(p, 1 - p)$ from the sigmoid output. In multi-task settings, the confidence is first computed for each task and then averaged to yield the final ID score. The reported OOD score is defined as $1 - \text{ID score}$.

Energy (Liu et al., 2020) uses the energy score defined as $E(x) = -\log \sum_c \exp(z_c)$, where z are the logits. For binary or single-output tasks, we augment the logits as $[z, -z]$ before computing the log-sum-exp. In the multi-task case, the energy is computed per task and then averaged. Larger energy values correspond to higher OOD likelihood.

ODIN (Liang et al., 2017) is implemented in our setting directly on the pre-computed molecular feature representations that serve as inputs to the classifier head, rather than on raw molecules. A small perturbation is applied according to $x' = x - \varepsilon \cdot \text{sign}(\partial \mathcal{L}_{\text{CE}} / \partial x)$, with $\varepsilon = 0.0014$. Temperature scaling with $T = 1000$ is applied exactly once to the logits. The model is kept in evaluation mode with Batch Normalization layers frozen. The confidence score is computed in the same way as MSP after perturbation, and task-level confidences are averaged in the multi-task case. The OOD score is then reported as $1 - \text{confidence}$.

Mahalanobis (Lee et al., 2018) operates in the penultimate feature space of the classifier head. For single-task classification, it estimates class-conditional means and a shared precision matrix, where Ledoit–Wolf shrinkage is used preferentially and empirical covariance is used as a fallback. The OOD score for a test sample is its minimum Mahalanobis distance to any class mean. In the multi-task setting, we instead fit a single global mean and a shared precision matrix, and the OOD score is given by the Mahalanobis distance to this global mean. Larger distances indicate higher OOD likelihood.

KNN (Sun et al., 2022) also works in the penultimate feature space, standardized using the mean and standard deviation of the training set. The OOD score is defined as the average Euclidean distance to the $k = 50$ nearest neighbors in this space. A larger average distance indicates that the sample is more likely to be OOD.

LOF (Breunig et al., 2000) is applied in the same standardized feature space. A Local Outlier Factor (LOF) model is fitted in novelty detection mode with $n_{\text{neighbors}} = 20$. The OOD score is defined as $-\text{score_samples}(\cdot)$, so that higher values correspond to samples that deviate more strongly from the local density of their neighbors.

C ADDITIONAL EXPERIMENTAL RESULTS

C.1 ANALYSIS OF TRAINING DYNAMICS

Self-Paced Learning Behavior. Across all three shifts, the dynamics match our theoretical analysis that the proposed Mole-PAIR prioritizes hard and borderline pairs. Concretely, both the misranked proportion $\Pr(\Delta E_\phi < 0)$ and the boundary mass $\Pr(|\Delta E_\phi| < \varepsilon)$ drop rapidly during the first

few epochs, while the mean margin $\mathbb{E}[\Delta E_\phi]$ increases steadily throughout training. This behavior is predicted by Eq. 9. Gradient updates are weighted by $w_\beta(\Delta) = \beta \sigma(-\beta \Delta)$, which is largest for misranked or borderline pairs and vanishes for already well-separated ones; hence the optimizer first fixes the pairs that most degrade AUROC and then spends diminishing effort on the rest.

Shift-Specific Dynamics. The three splits exhibit distinct rates of separation, consistent with our ablations: (i) **Size** corrects fastest: both error and boundary mass collapse early, and $\mathbb{E}[\Delta E_\phi]$ becomes large, indicating that size-based OOD is geometrically easy once the head has been trained. (ii) **Scaffold** improves steadily but more slowly, requiring more epochs to push borderline pairs away from the decision boundary—consistent with our β -sensitivity study, where Scaffold prefers a larger temperature (a sharper preference signal). (iii) **Assay** is the hardest: the misranked proportion diminishes but plateaus at a higher level; the boundary mass decreases more gradually; and the margin grows but remains comparatively small—again aligned with our observation that Assay favors a moderate β and weak regularization λ .

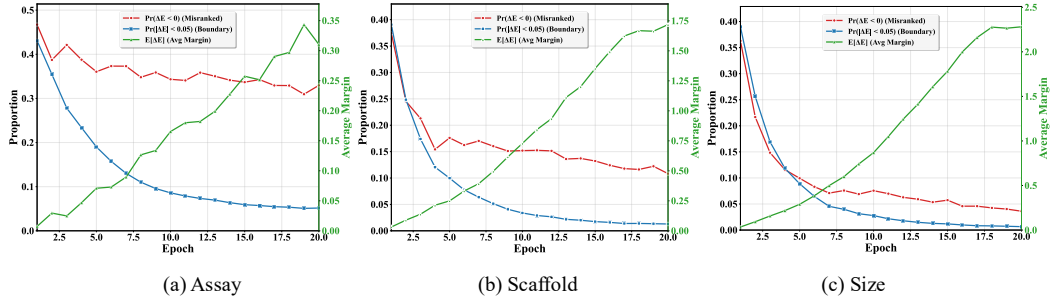


Figure 5: **Training dynamics of Mole-PAIR across three distribution shifts.** Each panel corresponds to one shift—(a) Assay, (b) Scaffold, (c) Size—and plots three metrics over 20 epochs: the misranked-pair proportion $\Pr(\Delta E_\phi < 0)$ (left y -axis), the boundary mass $\Pr(|\Delta E_\phi| < \varepsilon)$ with $\varepsilon = 0.05$ (left y -axis), and the average margin $\mathbb{E}[\Delta E_\phi]$ (right y -axis), where $\Delta E_\phi = E_\phi(S_{\text{out}}) - E_\phi(S_{\text{in}})$. The rapid decrease of the first two curves and the steady increase of the margin illustrate that hard or borderline pairs are corrected first.

C.2 GRADIENT WEIGHT ANALYSIS

Prioritization of Difficult Pairs. Across all shifts we observe the theoretically predicted ordering *Hard* > *Boundary* > *Easy* (Figure 6), with the boundary mean essentially equal to $w_\beta(0) = 0.05$. These ratios quantify the self-paced behavior predicted by Proposition 4.1: updates concentrate on misranked or borderline pairs (larger w_β) and spend little budget on already well-separated pairs (smaller w_β). The exact boundary level of 0.0500 further validates the loss in Eq. 6 and its gradient weighting in Eq. 20.

Shift-Specific Weight Distribution. Assay shows the smallest hard-over-easy advantage (+14.7%), indicating that many misranked pairs are only mildly negative, while easy pairs are not extremely far from the boundary. Scaffold exhibits a larger advantage (+28.4%), consistent with more well-separated easy pairs and hard pairs concentrated near the boundary. Size achieves the largest advantage (+32.4%) because easy pairs are very far from the boundary, whereas the remaining hard pairs are only slightly negative. This ordering mirrors the training dynamics and the β/λ sensitivity observed in the main text: Size splits are geometrically easy and quickly cleaned up; Scaffold benefits from a stronger preference signal; and Assay improves more gradually.

Implications for AUROC Optimization. Because AUROC equals $\Pr(E_\phi(S_{\text{ID}}) < E_\phi(S_{\text{OOD}}))$, the larger w_β on hard or borderline pairs ensures that training first reduces the mass of misordered pairs and then widens margins. This mechanism explains the down→down→up trajectories in Figure 5 and the strong test-time gains reported in Table 1 and Table 2.

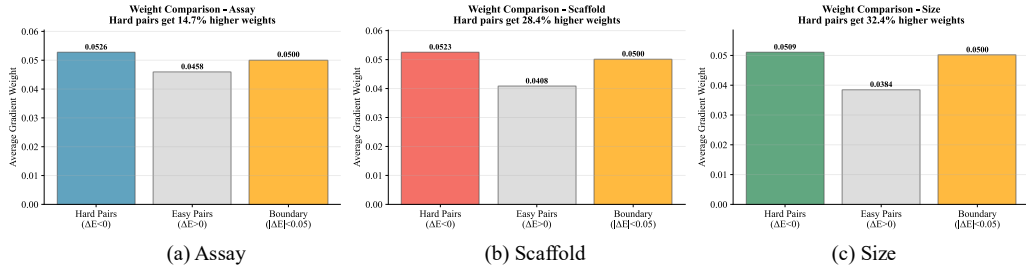


Figure 6: Hard vs. Easy vs. Boundary: average gradient weights across shifts. Bars show the mean of the per-pair update weight $w_\beta(\Delta) = \beta \sigma(-\beta\Delta)$ under three EC50 shifts (Assay, Scaffold, Size) with $\beta = 0.1$. Groups are: Hard pairs ($\Delta E_\phi < 0$), Easy pairs ($\Delta E_\phi > 0$), and Boundary pairs ($|\Delta E_\phi| < 0.05$).

Table 5: Model performance comparison: out-of-distribution detection results are measured by AU-ROC (\uparrow) / AUPR (\uparrow) / FPR95 (\downarrow) .

	Metrics	minimol						unimol								
		MSP	ODIN	Energy	Mah	LOF	KNN	Mole-PAIR	MSP	ODIN	Energy	Mah	LOF	KNN	Mole-PAIR	
EC50-Scaffold	AUROC	0.677 \pm 0.093	0.633 \pm 0.154	0.685 \pm 0.104	0.660 \pm 0.047	0.665 \pm 0.033	0.671 \pm 0.052	0.970 \pm 0.000	0.694 \pm 0.010	0.621 \pm 0.195	0.691 \pm 0.091	0.724 \pm 0.044	0.748 \pm 0.033	0.704 \pm 0.040	0.965 \pm 0.001	
	AUPR	0.627 \pm 0.081	0.597 \pm 0.108	0.625 \pm 0.096	0.696 \pm 0.034	0.690 \pm 0.026	0.700 \pm 0.050	0.975 \pm 0.000	0.692 \pm 0.009	0.660	0.646	0.681 \pm 0.086	0.717 \pm 0.006	0.763 \pm 0.034	0.696 \pm 0.050	0.972 \pm 0.000
	FPR95	0.725 \pm 0.109	0.734 \pm 0.128	0.716 \pm 0.111	0.898 \pm 0.023	0.893 \pm 0.025	0.870 \pm 0.042	0.178 \pm 0.010	0.848 \pm 0.070	0.816 \pm 0.115	0.849 \pm 0.083	0.831 \pm 0.033	0.844 \pm 0.088	0.855 \pm 0.018	0.178 \pm 0.008	
EC50-Size	AUROC	0.449 \pm 0.149	0.450 \pm 0.149	0.527 \pm 0.281	0.831 \pm 0.069	0.838 \pm 0.024	0.855 \pm 0.047	1.000 \pm 0.000	0.722 \pm 0.112	0.656	0.652 \pm 0.178	0.784 \pm 0.064	0.855 \pm 0.048	0.747 \pm 0.062	1.000 \pm 0.000	
	AUPR	0.455 \pm 0.098	0.453 \pm 0.086	0.541 \pm 0.204	0.834 \pm 0.055	0.847 \pm 0.022	0.853 \pm 0.039	1.000 \pm 0.000	0.697 \pm 0.116	0.652 \pm 0.131	0.655 \pm 0.035	0.726 \pm 0.068	0.849 \pm 0.058	0.691 \pm 0.064	1.000 \pm 0.000	
	FPR95	0.833 \pm 0.110	0.832 \pm 0.091	0.726 \pm 0.269	0.633 \pm 0.115	0.667 \pm 0.081	0.550 \pm 0.154	0.000 \pm 0.000	0.733 \pm 0.167	0.798 \pm 0.153	0.740 \pm 0.198	0.605 \pm 0.099	0.554 \pm 0.106	0.707 \pm 0.070	0.293 \pm 0.000	
EC50-Assay	AUROC	0.420 \pm 0.011	0.437 \pm 0.018	0.455 \pm 0.042	0.572 \pm 0.008	0.537 \pm 0.011	0.569 \pm 0.010	0.711 \pm 0.002	0.547 \pm 0.038	0.558	0.561 \pm 0.047	0.607 \pm 0.017	0.591 \pm 0.017	0.558 \pm 0.016	0.159 \pm 0.022	0.650 \pm 0.004
	AUPR	0.445 \pm 0.012	0.454 \pm 0.021	0.480 \pm 0.036	0.577 \pm 0.007	0.545 \pm 0.008	0.571 \pm 0.007	0.698 \pm 0.002	0.555 \pm 0.028	0.561	0.579 \pm 0.053	0.602 \pm 0.014	0.590 \pm 0.014	0.569 \pm 0.013	0.595 \pm 0.016	0.641 \pm 0.005
	FPR95	0.972 \pm 0.006	0.950 \pm 0.063	0.973 \pm 0.004	0.929 \pm 0.000	0.933 \pm 0.001	0.930 \pm 0.008	0.823 \pm 0.007	0.957 \pm 0.021	0.913 \pm 0.009	0.948 \pm 0.006	0.921 \pm 0.001	0.935 \pm 0.008	0.914 \pm 0.012	0.869 \pm 0.009	
IC50-Scaffold	AUROC	0.574 \pm 0.188	0.575 \pm 0.156	0.562 \pm 0.186	0.620 \pm 0.063	0.625 \pm 0.034	0.655 \pm 0.081	0.983 \pm 0.000	0.585 \pm 0.055	0.546	0.648 \pm 0.542	0.542 \pm 0.699	0.624 \pm 0.024	0.717 \pm 0.053	0.682 \pm 0.047	0.977 \pm 0.000
	AUPR	0.538 \pm 0.114	0.714 \pm 0.156	0.557 \pm 0.149	0.656 \pm 0.057	0.652 \pm 0.037	0.679 \pm 0.054	0.984 \pm 0.000	0.644 \pm 0.051	0.571	0.561 \pm 0.085	0.667 \pm 0.033	0.714 \pm 0.058	0.654 \pm 0.047	0.980 \pm 0.000	
	FPR95	0.759 \pm 0.126	0.563 \pm 0.25	0.781 \pm 0.117	0.909 \pm 0.037	0.909 \pm 0.013	0.898 \pm 0.030	0.084 \pm 0.005	0.926 \pm 0.034	0.945	0.935 \pm 0.033	0.818 \pm 0.034	0.832 \pm 0.046	0.833 \pm 0.049	0.139 \pm 0.008	
IC50-Size	AUROC	0.515 \pm 0.219	0.516 \pm 0.220	0.573 \pm 0.325	0.751 \pm 0.060	0.745 \pm 0.070	0.765 \pm 0.064	0.999 \pm 0.000	0.637 \pm 0.136	0.591	0.689 \pm 0.598	0.686 \pm 0.723	0.733 \pm 0.055	0.660 \pm 0.062	1.000 \pm 0.000	
	AUPR	0.494 \pm 0.199	0.495 \pm 0.190	0.593 \pm 0.250	0.763 \pm 0.061	0.753 \pm 0.001	0.776 \pm 0.001	0.999 \pm 0.000	0.642 \pm 0.142	0.625	0.675 \pm 0.593	0.682 \pm 0.683	0.736 \pm 0.059	0.757 \pm 0.016	0.615 \pm 0.071	1.000 \pm 0.000
	FPR95	0.743 \pm 0.192	0.741 \pm 0.194	0.662 \pm 0.268	0.786 \pm 0.073	0.803 \pm 0.068	0.782 \pm 0.088	0.004 \pm 0.000	0.861 \pm 0.137	0.911	0.881 \pm 0.072	0.707 \pm 0.178	0.707 \pm 0.070	0.746 \pm 0.106	0.809 \pm 0.080	0.000 \pm 0.000
IC50-Assay	AUROC	0.600 \pm 0.008	0.614 \pm 0.007	0.569 \pm 0.053	0.516 \pm 0.022	0.564 \pm 0.010	0.502 \pm 0.031	0.660 \pm 0.000	0.549 \pm 0.025	0.538	0.584 \pm 0.014	0.551 \pm 0.027	0.562 \pm 0.011	0.547 \pm 0.017	0.575 \pm 0.000	0.640 \pm 0.003
	AUPR	0.580 \pm 0.020	0.590 \pm 0.011	0.550 \pm 0.052	0.520 \pm 0.017	0.561 \pm 0.007	0.504 \pm 0.008	0.653 \pm 0.003	0.562 \pm 0.015	0.545	0.602 \pm 0.032	0.560 \pm 0.023	0.568 \pm 0.012	0.555 \pm 0.008	0.581 \pm 0.000	0.648 \pm 0.004
	FPR95	0.903 \pm 0.004	0.900 \pm 0.005	0.905 \pm 0.006	0.946 \pm 0.012	0.934 \pm 0.009	0.942 \pm 0.017	0.861 \pm 0.010	0.945 \pm 0.022	0.943	0.949 \pm 0.031	0.936 \pm 0.026	0.942 \pm 0.016	0.927 \pm 0.009	0.929 \pm 0.011	0.890 \pm 0.004
HIV-Scaffold	AUROC	0.408 \pm 0.004	0.390 \pm 0.005	0.388 \pm 0.037	0.503 \pm 0.028	0.508 \pm 0.024	0.562 \pm 0.066	0.777 \pm 0.000	0.465 \pm 0.113	0.415	0.499 \pm 0.076	0.476 \pm 0.112	0.567 \pm 0.013	0.594 \pm 0.015	0.580 \pm 0.028	0.728 \pm 0.000
	AUPR	0.438 \pm 0.014	0.430 \pm 0.030	0.423 \pm 0.021	0.497 \pm 0.009	0.499 \pm 0.018	0.538 \pm 0.049	0.740 \pm 0.000	0.489 \pm 0.009	0.474	0.481 \pm 0.092	0.490 \pm 0.047	0.547 \pm 0.017	0.576 \pm 0.010	0.450 \pm 0.024	0.708 \pm 0.008
	FPR95	0.953 \pm 0.002	0.962 \pm 0.028	0.955 \pm 0.017	0.947 \pm 0.016	0.943 \pm 0.014	0.906 \pm 0.003	0.624 \pm 0.009	0.954 \pm 0.018	0.947	0.922 \pm 0.002	0.952 \pm 0.028	0.920 \pm 0.001	0.894 \pm 0.021	0.885 \pm 0.021	0.736 \pm 0.011
HIV-Size	AUROC	0.194 \pm 0.136	0.336 \pm 0.317	0.167 \pm 0.122	0.919 \pm 0.059	0.889 \pm 0.034	0.921 \pm 0.055	1.000 \pm 0.000	2.181 \pm 0.088	0.278	0.216 \pm 0.243	0.214 \pm 0.826	0.286 \pm 0.080	0.282 \pm 0.226	1.000 \pm 0.000	
	AUPR	0.353 \pm 0.049	0.430 \pm 0.144	0.344 \pm 0.044	0.906 \pm 0.077	0.877 \pm 0.034	0.898 \pm 0.071	1.000 \pm 0.000	0.353 \pm 0.023	0.387	0.376 \pm 0.089	0.376 \pm 0.081	0.406 \pm 0.082	0.360 \pm 0.036	1.000 \pm 0.000	
	FPR95	0.983 \pm 0.082	0.819 \pm 0.248	0.985 \pm 0.028	0.315 \pm 0.144	0.458 \pm 0.084	0.280 \pm 0.130	0.001 \pm 0.000	0.985 \pm 0.033	0.977	0.982 \pm 0.022	0.514 \pm 0.072	0.567 \pm 0.113	0.563 \pm 0.000	0.000 \pm 0.000	
PCBA-Scaffold	AUROC	0.632 \pm 0.007	0.623 \pm 0.005	0.642 \pm 0.034	0.564 \pm 0.038	0.564 \pm 0.030	0.459 \pm 0.078	0.924 \pm 0.002	0.476 \pm 0.141	0.445	0.451 \pm 0.099	0.476 \pm 0.121	0.567 \pm 0.013	0.594 \pm 0.015	0.553 \pm 0.000	0.875 \pm 0.001
	AUPR	0.601 \pm 0.008	0.591 \pm 0.005	0.615 \pm 0.027	0.559 \pm 0.022	0.575 \pm 0.015	0.485 \pm 0.068	0.924 \pm 0.000	0.504 \pm 0.094	0.481	0.480 \pm 0.054	0.481 \pm 0.094	0.546 \pm 0.028	0.552 \pm 0.002	0.876 \pm 0.001	
	FPR95	0.883 \pm 0.004	0.856 \pm 0.084	0.852 \pm 0.085	0.922 \pm 0.026	0.934 \pm 0.012	0.960 \pm 0.015	0.348 \pm 0.001	0.954 \pm 0.080	0.962	0.984 \pm 0.054	0.836 \pm 0.284	0.948 \pm 0.026	0.941 \pm 0.001	0.515 \pm 0.009	
PCBA-Size	AUROC	0.697 \pm 0.073	0.691 \pm 0.065	0.735 \pm 0.091	0.728 \pm 0.119	0.687 \pm 0.156	0.527 \pm 0.160	1.000 \pm 0.000	0.350 \pm 0.236	0.353	0.353 \pm 0.253	0.350 \pm 0.258	0.690 \pm 0.090	0.607 \pm 0.096	0.668 \pm 0.006	1.000 \pm 0.000
	AUPR	0.654 \pm 0.087	0.657 \pm 0.086	0.700 \pm 0.117	0.713 \pm 0.120	0.696 \pm 0.147	0.519 \pm 0.093	1.000 \pm 0.000	0.455 \pm 0.168	0.456	0.416 \pm 0.455	0.416 \pm 0.455	0.689 \pm 0.084	0.639 \pm 0.100	0.684 \pm 0.081	1.000 \pm 0.000
	FPR95	0.698 \pm 0.134	0.763 \pm 0.068	0.697 \pm 0.134	0.752 \pm 0.137	0.804 \pm 0.158	0.902 \pm 0.128	0.001 \pm 0.000	0.925 \pm 0.157	0.925	0.857 \pm 0.157	0.855 \pm 0.068	0.926 \pm 0.073	0.893 \pm 0.009	0.809 \pm 0.000	1.000 \pm 0.000
ZINC-Scaffold	AUROC	0.359 \pm 0.004	0.360 \pm 0.008	0.359 \pm 0.034	0.638 \pm 0.011	0.544 \pm 0.056	0.636 \pm 0.030	0.614 \pm 0.004	0.352 \pm 0.114	0.350	0.352 \pm 0.114	0.350 \pm 0.114	0.643 \pm 0.113	0.577 \pm 0.041	0.641 \pm 0.095	1.000 \pm 0.000
	AUPR	0.346 \pm 0.008	0.416 \pm 0.016	0.416 \pm 0.043	0.637 \pm 0.010	0.508 \pm 0.047	0.637 \pm 0.037	0.587 \pm 0.004	0.437 \pm 0.099	0.437	0.436 \pm 0.047	0.436 \pm 0.047	0.694 \pm 0.048	0.610 \pm 0.042	0.670 \pm 0.036	1.000 \pm 0.000
	FPR95	0.985 \pm 0.003	0.985 \pm 0.003	0.985 \pm 0.003	0.905 \pm 0.023											